SEMARAK ILMU PUBLISHING

CFD Letters

Journal homepage:
https://semarakilmu.com.my/journals/index.php/CFD_Letters/index
ISSN: 2180-1363

Numerical Study of Comparison of Thrust Bearing Slip - No Slip Condition on Acoustic Performance

Imam Syafaat[1,2,*], Luky Rika Sari[1], Muchammad Muchammad[1], Mohammad Tauviqirrahman[1], Eflita Yohana[1], Jamari Jamari[1], Budi Setiyana[1,3]

[1] Department of Mechanical Engineering, Faculty of Engineering, Diponegoro University, Jl. Prof Sudarto SH Tembalang 50275, Semarang, Indonesia
[2] Department of Mechanical Engineering, Faculty of Engineering, Universitas Wahid Hasyim, Jl. Menoreh Tengah X/22 Sampangan 50236, Semarang, Indonesia
[3] Laboratory for Surface Technology and Tribology, Faculty of Engineering Technology, University of Twente, Drienerloolan 5, Postbox 217, 7500 AE, Enschede, Netherlands

ARTICLE INFO

Article history:
Received 9 February 2023
Received in revised form 10 March 2023
Accepted 8 April 2023
Available online 1 September 2023

Keywords:
Thrust Bearing; Slip; Acoustic; CFD

ABSTRACT

The acoustic power level (APL) produced by a thrust bearing during operation has a major effect on its performance. Therefore, this research aimed to investigate the impact of slip engineered on the noise generated by thrust bearings. A numerical approach was used to simulate open pocket bearings with varying film thickness depths. At the initial location of the slip area, three bearing models were analyzed: pocket slip, pocket no slip, and smooth slip. The results show that implementing slip can reduce noise levels, turbulence kinetic energy (TKE), and turbulence eddy dissipation (TED) rate. The average APL, TKE, and TED values were the lowest at the high film thickness.

1. Introduction

Bearing is designed to minimize friction in a mechanical system. One type of bearing is the thrust bearing, which supports axial movement in the direction of the shaft axis. Subsequently, recent advancements in thrust-bearing research have focused on incorporating artificial surface textures, such as textures, pockets, grooves, or dimples, to enhance performance texture. These surface textures, friction, load support, temperature, and noise have a beneficial impact.

The use of surface textures in thrust bearings can reduce the frictional force or frictional coefficient and improve bearing performance, as evidenced by various investigations [1-13]. Research by Rahmani *et al.,* [14] showed that increasing the number of dimples would not help reduce the friction coefficient. This implies that there are optimal conditions regarding the number of dimples that benefit the bearing.

The use of software such as Computational Fluid Dynamics (CFD) has become common in predicting bearing performance [15-20], with many CFD based research providing satisfactory results

* *Corresponding author.*
E-mail address: imamsyafaat@unwahas.ac.id (Imam Syafaat)

https://doi.org/10.37934/cfdl.15.9.117

when validated against experiments [21-22]. Furthermore, Fouflias *et al.,* [4] modeled four types of thrust bearings: tapered land, open pocket, closed pocket and textured. The effects of varying the depth of each geometry pattern were investigated. The results of the analysis showed that open-pocket bearings have the greatest load support compared to other types. The textured bearing has the lowest coefficient of friction with low loads and rotation. The research above ignores slippage, and one method for increasing a bearing's load support is to create a slip effect on the bearing surface, as described in research [23-28].

Low noise, represented by the APL generated by friction between the fluid and other parts, is as important as identifying good bearing performance. The APL has a significant impact on bearing performance because it is an interpretation of the vibrations generated when the thrust bearing is in operation. Research by Lu and Khonsari [29] and Meng and Zhang [30] described how surface roughness affects the noise in journal bearings. Furthermore, Meng *et al.,* [31] used CFD to investigate the level of acoustic power as depth, width, and dimple position varied. According to their investigation, the size and placement of dimples must be carefully chosen to simultaneously reduce the noise between these two factors. When the dimple is present, there is a relationship between noise fluctuations and film pressure. When the dimple is placed in an area with high fluid pressure, there is a relationship between noise fluctuations and film pressure. Meng *et al.,* [32] investigated the isothermal and thermal condition of journal bearing with compound texture. Muchammad *et al.,* [33] recently investigated speed variations in no slip multi-step journal bearings with a certain eccentricity. They found that the higher the liquid velocity, the higher the resulting hydrodynamic pressure, vapor volume fraction, temperature, and APL. Meanwhile, in terms of slip engineered in journal bearings, Tauviqirrahman *et al.,* [34] reported that surfaces with heterogeneous conditions (slip and no slip) can increase the load support by two times compared to conventional bearings. When compared to conventional bearings, this slip effect can reduce the temperature by up to a quarter.

According to the literature review, knowing the slip location placement can alter the acoustic and tribological performance. If the slip is located in an unfavorable location, it can degrade tribological performance. That is why we are concentrating on how to determine the slip location. Many researchers have examined surface texture to determine the performance of thrust bearings, but research on combining the slip and open pocket thrust bearing according APL is still very limited. Under these conditions, in this study, the slip was applied in pocket areas and on smooth surfaces to determine bearing performance, specifically acoustic power level (APL), turbulence kinetic energy (TKE), and turbulence eddy dissipation rate (TED). The APL is related to noise. Noise indicates excessive friction between the lubricant and the bearing surface. The low noise level indicates that the bearing friction less. The machine's service life will be extended if the friction is avoided. The use of computer programs to simulate fluid conditions, on the other hand, can identify bearing performance behavior. According to the statement above, it is necessary to examine the impact of this slip on the noise produced. In this research, the resulting APL was analyzed using modeling based on CFD open pocket bearings. Furthermore, the type of open pocket bearing refers to the geometry of Fouflias *et al.,* [4], which produces a high load support. This investigation also examines both the TKE and TED.

2. Methodology

2.1 Governor Equations

In order to describe the fluid noise in the pocket bearing, the Reynolds-Averaged N-S (RANS) equation for incompressible viscous fluid is employed to obtain the lubrication film pressure expresses as Eq. (1).

$$\frac{\partial}{\partial x_j}(\rho u_i u_j) = -\frac{\partial p}{\partial x_j} + \frac{\partial}{\partial x_j}\left[\mu\left(\frac{\partial u_i}{\partial x_j} + \frac{\partial u_j}{\partial x_i}\right)\right] + \frac{\partial}{\partial x_j}(-\rho\overline{u'_i u'_j}) \tag{1}$$

where $u_i(u_j)$ denoted the average speed of fluid along the coordinate $x_i(x_j)$ and for the lubricant with density ρ and dynamic viscosity μ, its average film pressure is *p* as well as its fluctuating velocity in the *i*-direction is denoted by $u_i prime$. The Reynolds stress is denoted by $-\rho\overline{u'_i u'_j}$ can be expressed as Eq. (2).

$$-\rho\overline{u'_i u'_j} = \mu\left(\frac{\partial u_i}{\partial x_j} + \frac{\partial u_j}{\partial x_i}\right) - \frac{2}{3}\left(\rho k + \mu t \frac{\partial u_i}{\partial x_i}\right)\delta_{ij} \tag{2}$$

where $\overline{u'_i u'_j}$ is fluctuating velocity, δ_{ij} is Kronecker from the delta symbol. If *i=j*, δ_{ij} =1. Otherwise, if $i \neq j$, δ_{ij} = 0, the turbulent viscosity coefficient μ_t is defined as $\mu_t = C_\mu \rho k^2/\varepsilon$

$$W = a_\varepsilon \rho \left(\frac{u_i^3}{l}\right)\frac{u_i^5}{c_0^5} \tag{3}$$

$$L_p(dB) = 10\log\left(\frac{W}{W_{ref}}\right) \tag{4}$$

The turbulent flow in the pocket creates noise during operation. For noise analysis, Eq. (3) is used to calculate the acoustic power per unit volume (*W*). In this equation, c_0 is the sound speed in lubricant, which is assumed to be 1480 m/s [31], *l* is the turbulent length, determined by flow field characteristics, *k* is the turbulence kinetic energy, and ε is the turbulence eddy dissipation rate. The last, the APL (L_p) of the bearing noise is obtained as Eq. (4) where the referenced acoustic power W_{ref} is assumed to be 10^{-12} W/m^3 [36]. In this research, it should be noted that Ansys FLUENT [37] was used to solve all equations.

2.2 Fluid Flow Modeling

Thrust bearing are made up of three major components, the stator, fluid, and rotor. Figure 1 shows the hydrodynamic thrust bearing components used with eight pockets, only one of which was simulated. The rotor is the upper half of the bearing, while the stator or pad is the lower, static component. The geometry of the bearing has outer (D_o) and inner (D_i) diameters of 90 mm and 50 mm, respectively. In this research, the stator geometry used was not novel and was similar to the previous investigation [4]. However, the novelty was based on the presence of slip. The inner (D_{pi}) and outer (D_{po}) diameters of the pocket are 55 and 85 mm, respectively.

The length of the pad in the mid sector was 24.49 mm, and the pocket length (L_p) determined the diameter location. The angle of the pocket area (a_p) was 29°, while the length of the pocket (B_p) was 15 mm. The minimum film thickness (H_{min}) varies, i.e., 15, 20, 30, 50, and 80 μm. The pocket depth

(H_d) of 20 μm, on the left and right, there are grooves with a width (L_g) and depth of 3 mm and 4 mm, respectively. The top fluid (U) moves at a constant speed, while the bottom pocket has slip conditions.

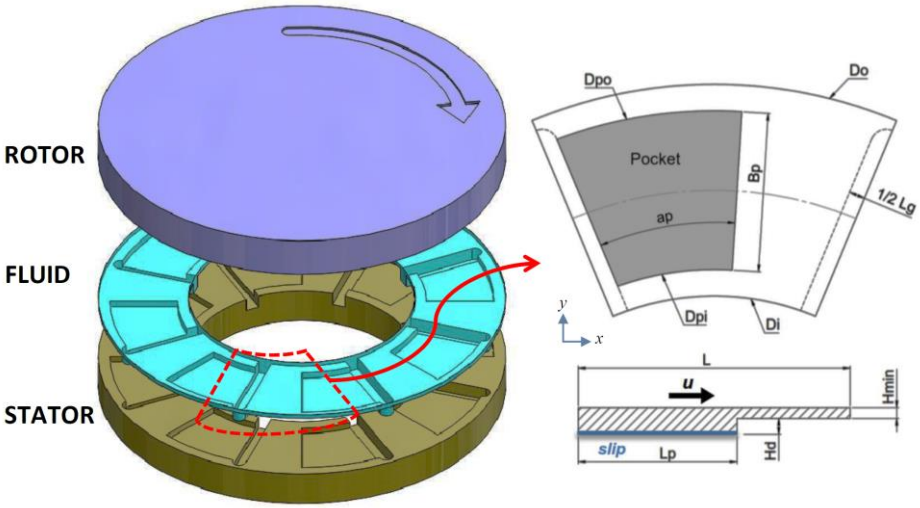

Fig. 1. An open pocket thrust bearing with eight pockets, only one of which is simulated in this study

The boundary conditions of the simulation are shown in Figure 2. It has been found that fluid enters the bearing both through the inner surface and through the grooves on either side of the pad. The fluid temperature was set to 40 degrees Celsius, and the inlet oil pressure was assumed to be constant at 0.1 MPa (1 atm), see Figure 2 for these locations. In addition, the outer fluid surface was designed as an outlet with a pressure of 0 MPa. The rotor interface and stator contact occupied the top and bottom surfaces, respectively. Because the top lubricant was affected by rotor rotation, temperature continuity, and heat flux, the groove was designed to be periodic on both sides. In the pocket, the slip condition was designed. In this simulation, the speed was set to 2000 rpm for all H_{min} in the stator section, while the other parts were set to no slip. In this research, the assumptions were steady and incompressible flow conditions, but the heat conduction in the rotor and stator was not taken into account.

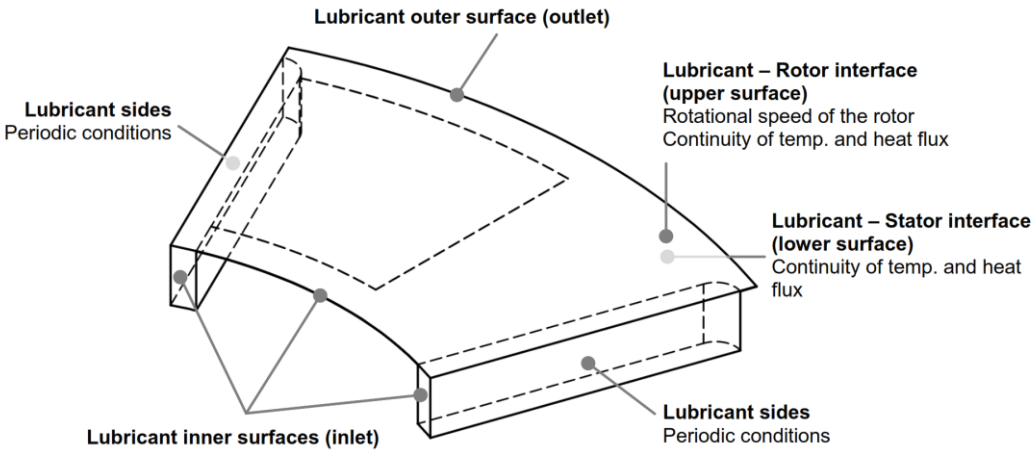

Fig. 2. An illustration of the fluid domain's boundary conditions

To provide water vapor concessions, this simulation uses the mixed phase method of the Ansys FLUENT function. The properties of the water used in this simulation are presented in Table 1. In this research, some of the parameters are based on the article by Meng and Zhang [30]. Broadband noise sources with a reference acoustic power of 1E-12 must be activated to detect acoustic modeling. Similarly, the setting for Far-field sound speed and the number of Fourier modes. While the SIMPLE scheme was used to set the solution methods and pressure was set to PRESTO!, and Turbulent Kinetic Energy was set to upwind first order. ICEM was used to mesh the geometry and the total number of meshing elements is about 900,000. The grid independence test for this meshing (see Figure 3) shows that changes in the number of elements after 1.0E+06 or larger cause a small change (under 0.20%) in the performance value (minimum pressure). This indicated the continuation of the various stages where the slip/no slip simulation in this study will be performed.

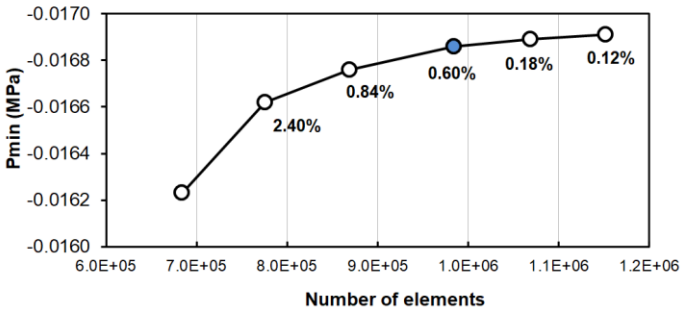

Fig. 3. Grid independence test of this simulation

As shown in Figure 4, the modeling is divided into three cases, pocket no slip, pocket slip, and smooth slip. Subsequently, a pocket no slip condition is one in which pockets and other locations do not receive a slip. Pocket slip is the condition that allows slipping in the pocket area, while the smooth slip is modeled on a thrust bearing that does not have a pocket but allows slipping in an area that is the same size as the pocket area. The third simulation aims to compare the effects of pocketed thrust bearings in the first and second cases with conventional thrust bearings without pockets.

Table 1
Properties of fluid in the present work

Parameter	Symbol	Value	Unit
Water viscosity	μ_o	0.001003	Pa.s
Water density	ρ_o	998.2	kg/m^3
The viscosity of water vapor	μ_v	1.34 x 10^{-5}	Pa.s
The density of water vapor	ρ_v	0.5542	kg/m^3
Saturation pressure of the vapor	P_v	4240	Pa

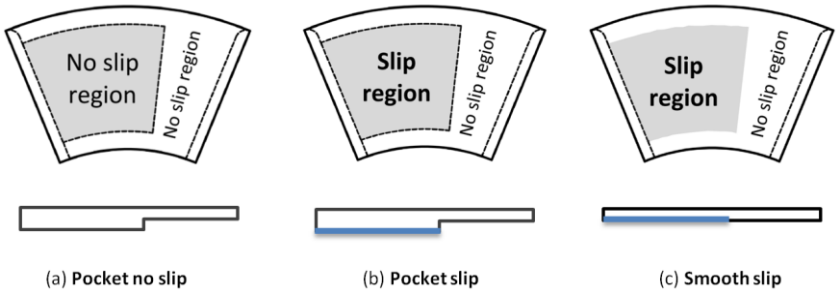

Fig. 4. The simulation of thrust bearing acoustic performance in slip and no slip situations

The model was developed by Fouflias *et al.,* [4], and validated, before running the simulation. The rotational speed in this simulation is 2000 rpm, with a bearing geometry of H_{min} 15 μm and H_d 20 μm. The inlet pressure is set to 0.1 MPa, and the inlet temperature is set to 40 °C. The density of the oil lubricant used is 870 kg/m^3. All parameter settings are based on the work of Fouflias *et al.,* [4].

Figure 5 shows the results of this model comparison. There is no noticeable difference between the two models where the highest pressure is at the end of the pocket. This is understandable as the transition area between pockets and no pockets has narrowed. The pressure then dissipates around the pocket area.

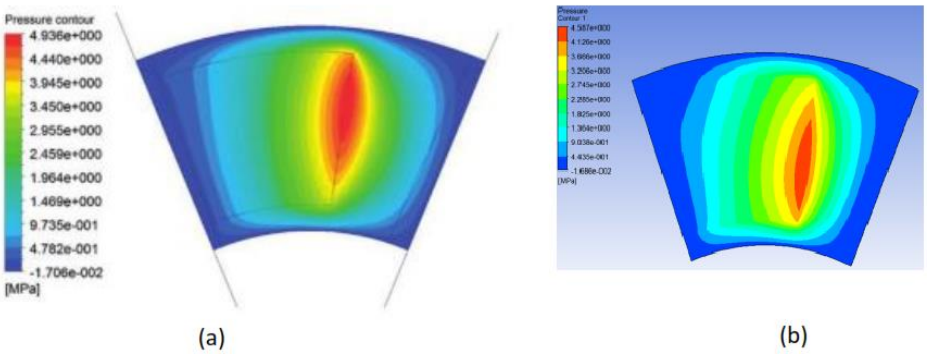

Fig. 5. Comparison of the pressure distribution in (a) Fouflias *et al.,* [4], and (b) present model

Figure 6 compares the appropriate load support in the current research to the previous investigation. To determine the load support behavior, all variations of H_{min} are simulated in this test. As shown, the current model has a deviation of less than one percent when compared to previous research. The greater the thickness of the film layer, the lower the resulting load support.

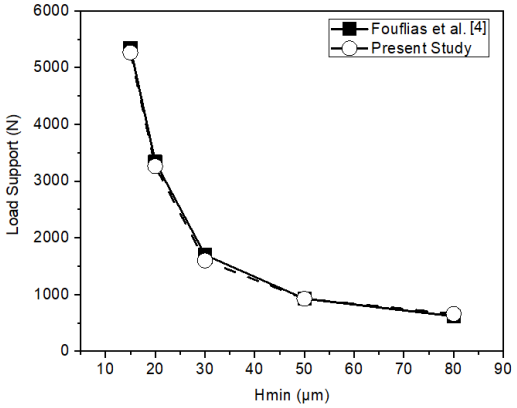

Fig. 6. Load support comparison between reference [4] and the present study

3. Results and Discussion

3.1 Acoustic Power Level (*APL*)

The APL is the amount of sound produced by friction in a fluid. Figure 7 shows the APL behaviour of the three models with different H_{min} values. In the pocket no slip model (Figure 7(a)), it can be seen that with small film thickness, the noise generated is higher and vice versa. There is fluctuating noise at x=0.004 μm because that is the beginning of the pocket. This data is collected horizontally at the

beginning of the pocket and in the centre. This is carried out at the beginning to detect the effect of pockets and slip engineered.

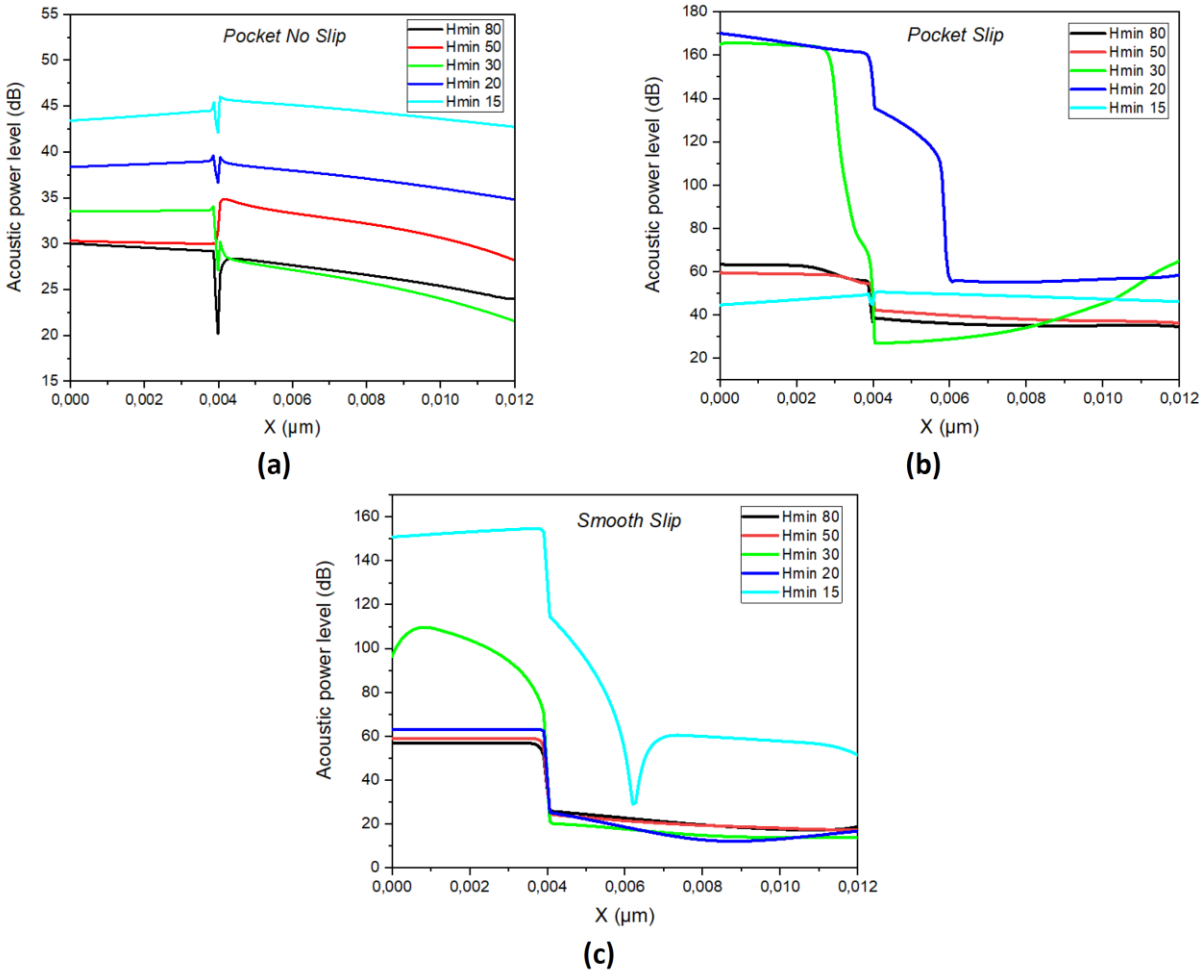

Fig. 7. The APL behavior between pocket no slip, pocket slip, and smooth slip models

In general, the noise decreases from the beginning of the pocket and then decreases, but at H_{min} 50 mm, the noise increases when it enters the pocket. When the lubricant flows through the pocket, it causes sudden changes in the film thickness. This is why the APL fluctuates. This shift in the APL is in line with Meng *et al.,* [30]. The APL rises in comparison to the initial position, particularly at H_{min} 50 and 80. The noise generated in the pocket slip case (Figure 7(b)) is less than 70 dB for H_{min} 15, 50, and 80, but for H_{min} 20 and 30, the noise increases by nearly 200 % compared to the initial position. The noise generated by the matched surface of the bearing (approx. 50-80 dB) in application may be harmful to people's hearing. In the smooth slip case (Figure 7(c)), the resulting noise decreases significantly from the beginning of the slip area. This research demonstrates that slip can reduce noise, but the resulting noise is significantly higher than in the no slip model. In this study, the largest noise fluctuation upon entering the pocket occurs at H_{min} 80 in the no slip case (Figure 7(a)). This is due to the fluid experiencing turbulence. Following this phase, the APL of the fluid decreases. The most possible explanation is that a large amount of fluid is going to rub against the surface of the pocket. This is what causes such large fluctuations in APL.

Figure 8 compares the three models that show the same variation in film thickness. The pocket models, both pocket no slip and pocket slip, show the same trend at H_{min} 15. The result of this phenomenon (see Figure 8(a)) is that the noise for the smooth slip model is classified as "very high",

almost four times the pocket model. It should be noted that the pocket model does not bring a noise reduction effect to H_{min} 15. The advantage of smooth slip modeling is that H_{min} 15 can reduce noise when entering the slip area by 60%. This generates noise of about 170 dB for both H_{min} 20 and 30. Slip can reduce noise by nearly 40% in the smooth slip model at H_{min} 50 (see Figure 8(d)). Of the three models, pocket no slip was found to be the most "stable" in noise at a variety of H_{min}. Meanwhile, when compared to the other two models, the smooth slip model has the lowest noise. Providing a slip can also reduce noise by 67% at H_{min} 20, and 83% at H_{min} 30, respectively for the pocket slip model. A lower APL does not always imply a thicker film layer, and vice versa. Fluid flow caused by turbulence has a variety of effects.

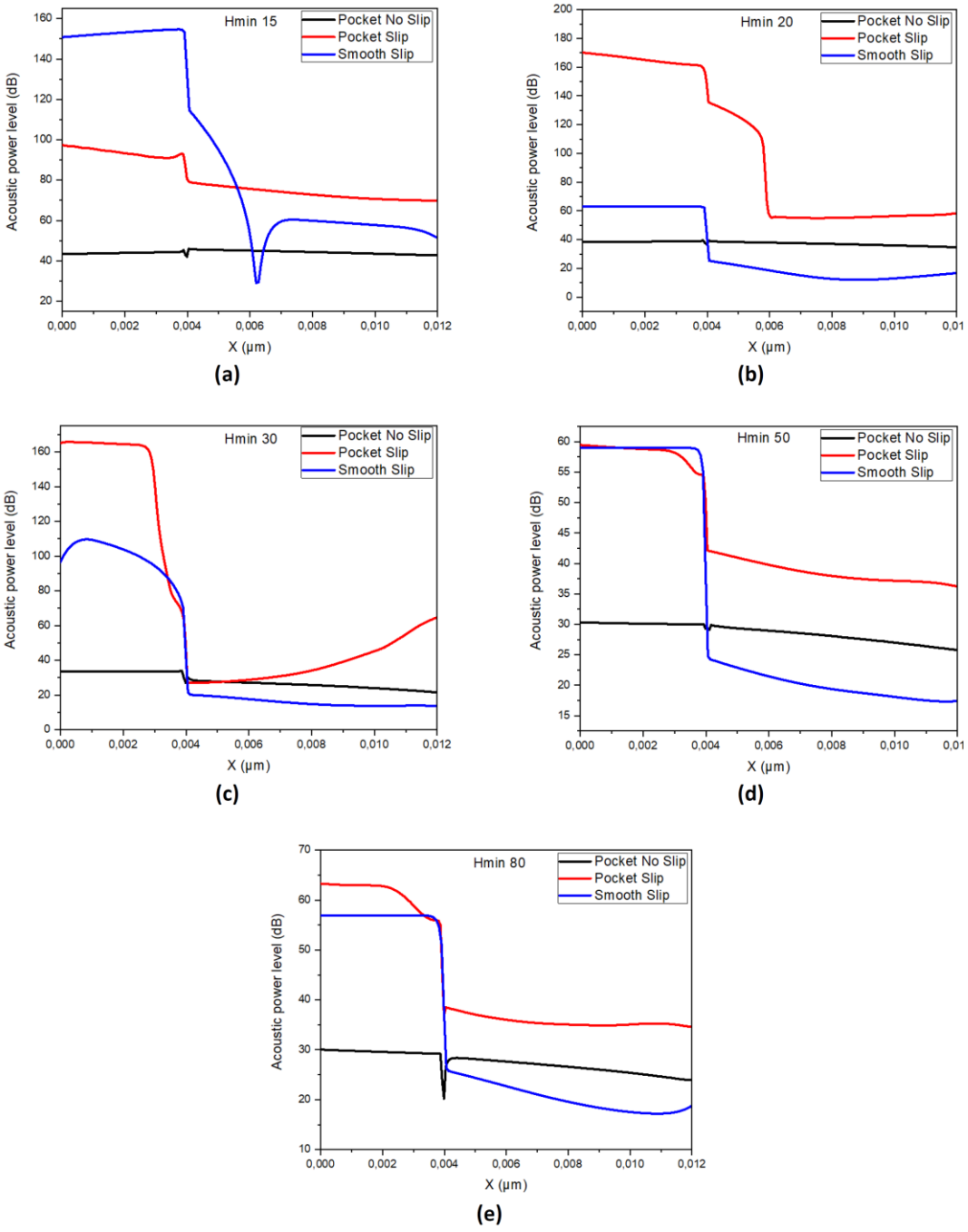

Fig. 8. APL comparison of H_{min} 15, 20, 30, 50, and 80 μm

Figure 9 shows the average APL of the three models. Of all H_{min} variations, the pocket no slip model has the lowest noise compared to other models. Therefore, the slip model, which includes both the pocket and smooth surface models, produces more noise. The smooth slip bearing decreases significantly at H_{min} 30 m. This trend is similar to the no slip pocket model, but the lowest APL at H_{min} 80 is 27.44 dB. Additionally, it can be seen that the smooth slip model has the highest average APL at H_{min} 15. Because the values are not significantly different at H_{min} 30, there is no significant difference in the average APL between the two slip models (pocket and smooth surface). In this case, the slip engineered has no effect on the noise that occurs. The possible explanation for this might be that the difference between minimum film thickness and pocket height is nearly identical. As a result, the effect of turbulence does not play a significant role in this case.

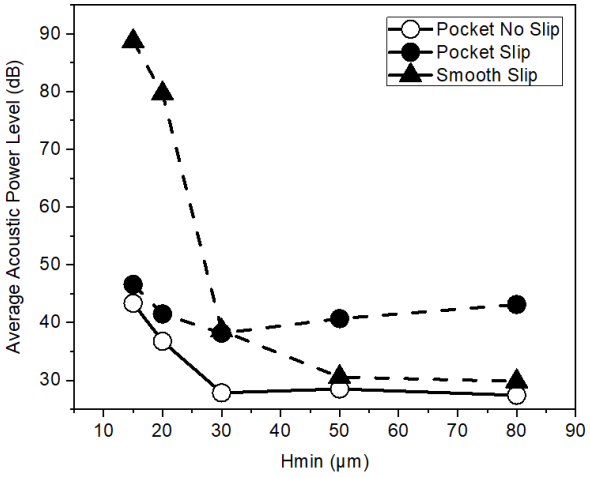

Fig. 9. The average APL comparison of H_{min} 15, 20, 30, 50, and 80 µm of pocket no slip, pocket slip, and smooth slip models

3.2 Turbulence Kinetic Energy (*TKE*)

Figure 10 illustrates the behaviour of TKE in three models with different H_{min} values. As shown, the pocket no slip model has a lower TKE range than the other models. H_{min} 15 (Figure 10(a)) produced the highest TKE upon entering the pocket in the no slip pocket model, followed by H_{min} 20 and 30. H_{min} 50 and 80 appear to have similar values before entering the pocket, but there is a difference in behaviour after entering the pocket. At H_{min} 50, the value increased by 28%, from 7.00E+07 J/kg before entering the pocket to 8.95E+07 J/kg after entering the pocket. It decreased when entering the pocket at H_{min} 80, as seen later. At H_{min} 80, it decreased when entering the pocket, then increased to as high as TKE when entering the pocket. In the pocket slip model (Figure 10(b)), the TKE value decreases when entering the pocket for all H_{min} variations. At H_{min} 20, the highest value is generated and then decreases as it enters the pocket. In comparison to other film thicknesses, the pocket slip model has a very large value difference between H_{min} 20 and 30 compared to the no slip pocket model. The smooth slip model in Figure 10(b) also exhibits a very large value difference between H_{min} 20 and 30. TKE is closely related to APL, see Eq. (1) to Eq. (3). In the general point of view, as TKE decreases, the fluctuation of lubricant velocity and subsequent bearing noise diminishes. As a result, the above TKE variation is understandable. This study's findings are consistent with Ref. [31].

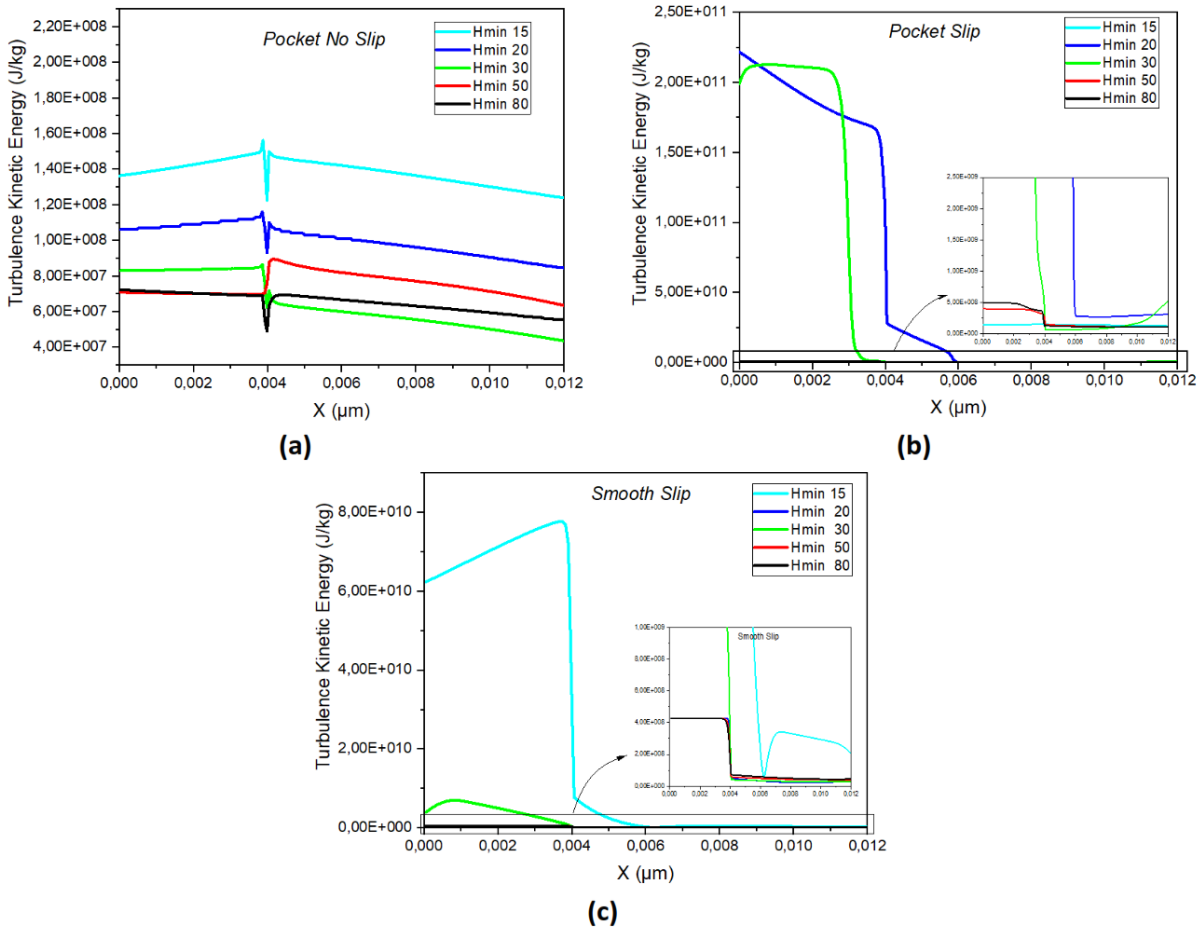

Fig. 10. The TKE behaviour between pocket no slip, pocket slip, and smooth slip models

Figure 11 demonstrates the TKE for all H_{min} variants. Apart from H_{min} 15, the smooth slip model has the lowest H_{min} TKE due to the turbulent flow entering the slip area. With the exception of the H_{min} 15, the pocket slip model produced the highest TKE of the researched cases. In general, it can be concluded that providing pockets from x=0.004 μm reduces the TKE value. An important point to note in this modeling is that the pocket no slip model, like APL, has the lowest fluctuations when compared to other models. Furthermore, H_{min} 80 has the lowest TKE in this research. TKE is highest before entering the pocket area in the pocket slip model at H_{min} 20 and 30, then decreases dramatically after entering the pocket. More than 80% of its TKE is accounted for by this reduction. At H_{min} 20 and 30 (see Figures 11(b) and (c)), the phenomenon of decreasing TKE when entering the pocket appears in the pocket slip model, but then increases again. The smooth slip case (Figure 11(a)) exhibits a similar trend at H_{min} 15. The existence of a decrease followed by an increase is not the same as the phenomenon observed in APL. Even for H_{min} 20 on the pocket slip model (Figure 8(d)), APL seems stable after entering the pocket. In generally speaking, there seems to be a trend toward similarity in TKE and APL behaviours in each H_{min}. The lower the generated APL, the lower the TKE produced, and vice versa. This linear relationship between APL and TKE in this study is in line with the research in Ref. [35].

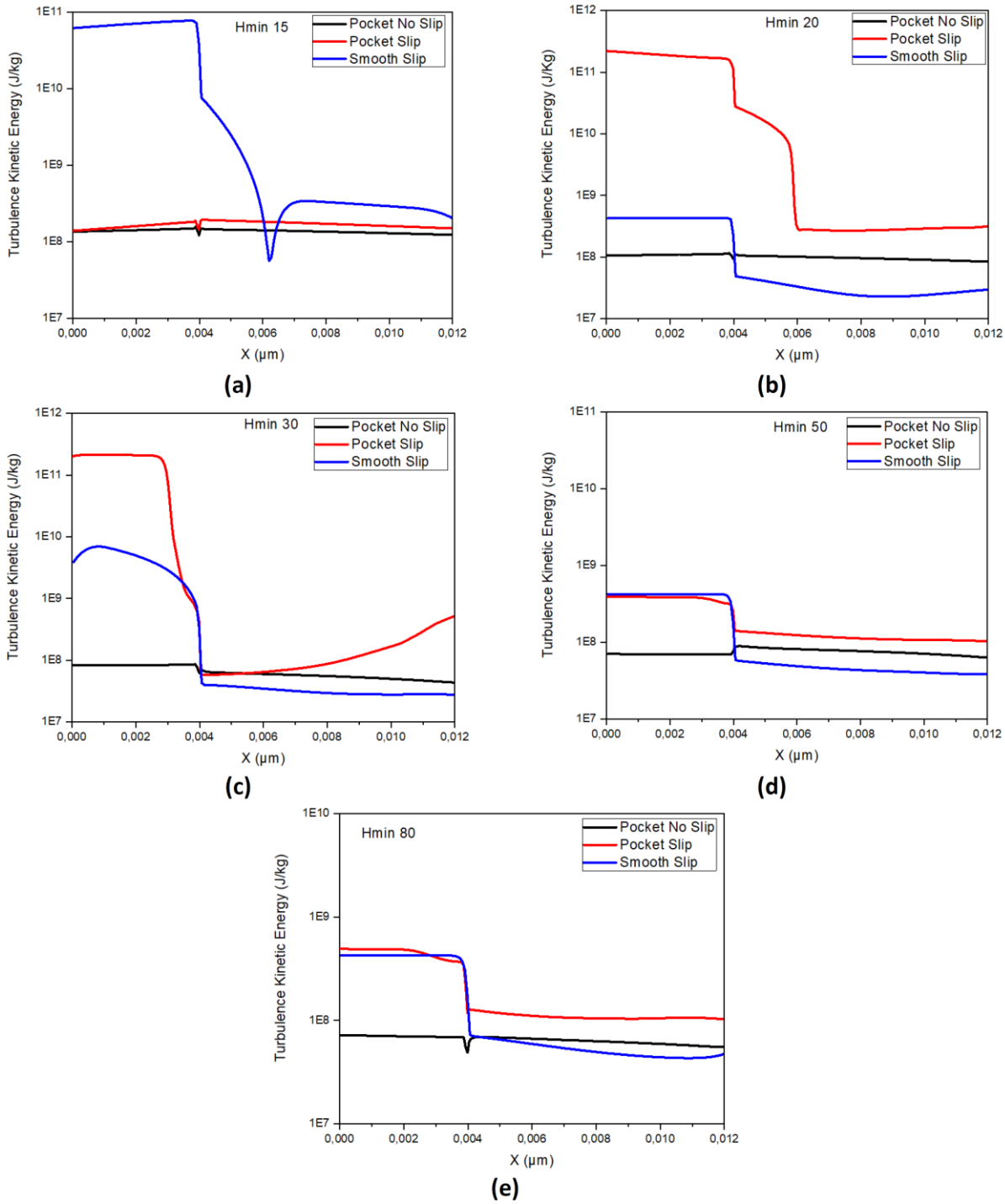

Fig. 11. The TKE comparison of H_{min} 15, 20, 30, 50, and 80 µm

Figure 12 depicts the average TKE produced. Of all H_{min} variations, the pocket no slip model has the lowest TKE value. The slip modelling (pocket and smooth surface) at Hmin 20 was found to have an average TKE greater than H_{min} 15. The lowest TKE value in all models was 7.34E7 J/kg at H_{min} 80. In general, TKE is directly proportional to APL compared to the average APL produced, and the higher the APL, the higher the TKE. This applies to all models on all H_{min} variations. In general, providing the slip can reduce the TKE. The presence of pockets on bearings has been proven to reduce both APL and TKE. The TKE generated from this simulation generally shows consistency with the APL results as in Figure 9. This is because the flowing fluid has an APL which is affected by TKE. The correlation can be seen in Eq. (1) to Eq. (3).

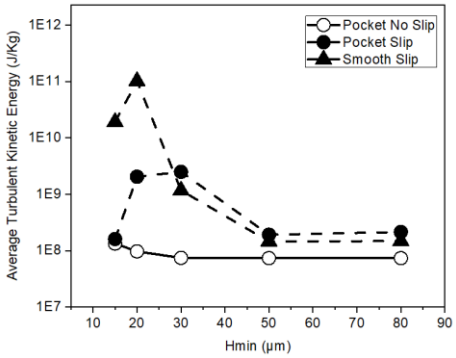

Fig. 12. The average TKE comparison of H_{min} 15, 20, 30, 50, and 80 µm of pocket no slip, pocket slip, and smooth slip models

3.3 Turbulence Eddy Dissipation (*TED*) *Rate*

Figure 13 shows a comparison of the three TED behaviour models. Compared to other models, the pocket no slip model has a distinct behavioural pattern. In contrast to the no slip model, the pocket slip and smooth slip models experience a decrease when entering the slip area. This research demonstrates that slip can reduce TED in all variations of H_{min} by excluding H_{min} 30 in the pocket no slip. The pocket no slip and smooth slip models have the highest TED values at H_{min} 15 is also seen in APL (Figure 7) and TKE (Figure 10). The consistency of the three behaviours is evident, as shown in Eq. (1) to Eq. (3). The logical explanation for H_{min} 15 is that the volume of the lubricating layer is deemed insufficient to dampen the noise in the pocket due to the high TKE and TED.

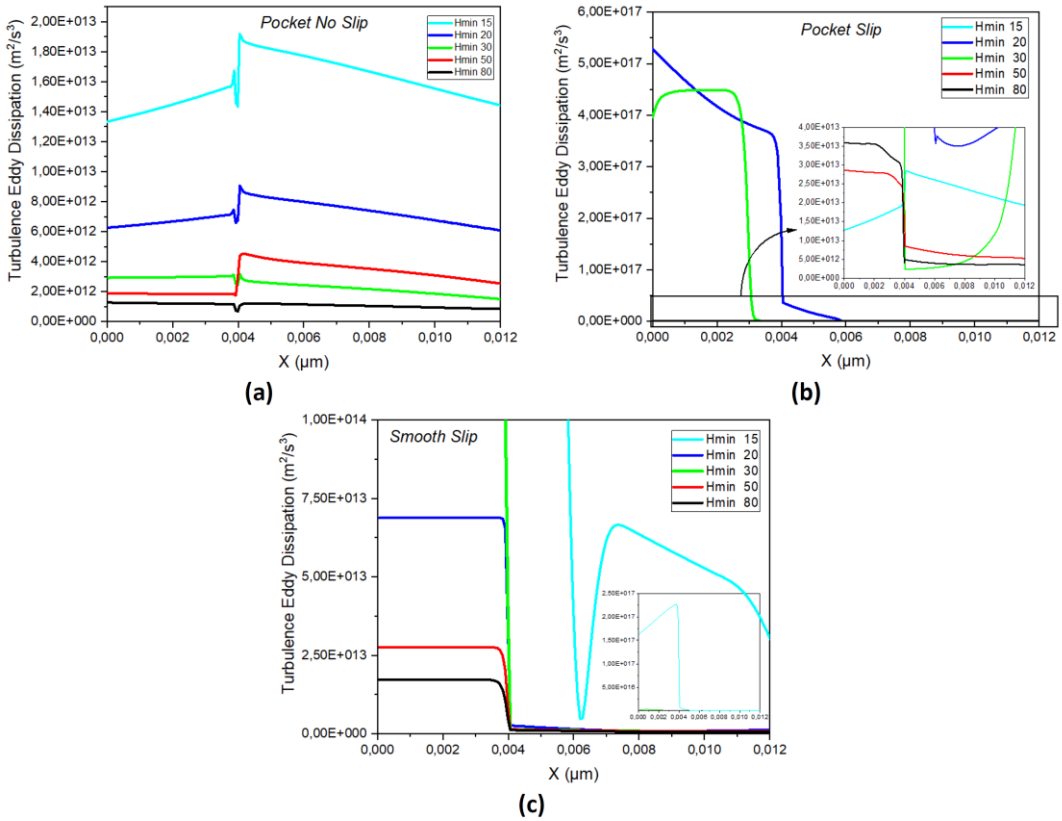

Fig. 13. The TED rate between pocket no slip, pocket slip, and smooth slip models

Figure 14 illustrates the TED in the three models for each H_{min} variation. In general, all TEDs in the smooth slip model decrease for all variations of H_{min} at x=0.004 μm, where the slip region begins. Figure 13(c) shows the pocket slip model's TED decreasing at H_{min} 30 and then increases. This is comparable to APL (Figure 8(c)) and TKE (Figure 11(c)). This means that TED, APL, and TKE have a mutually influencing relationship in the pocket slip model. The TKE and TED values increase as the APL value increases. The relationship between APL, TKE, and TED is once again interrelated. This is also consistent with the findings of Ref. [32] and [35].

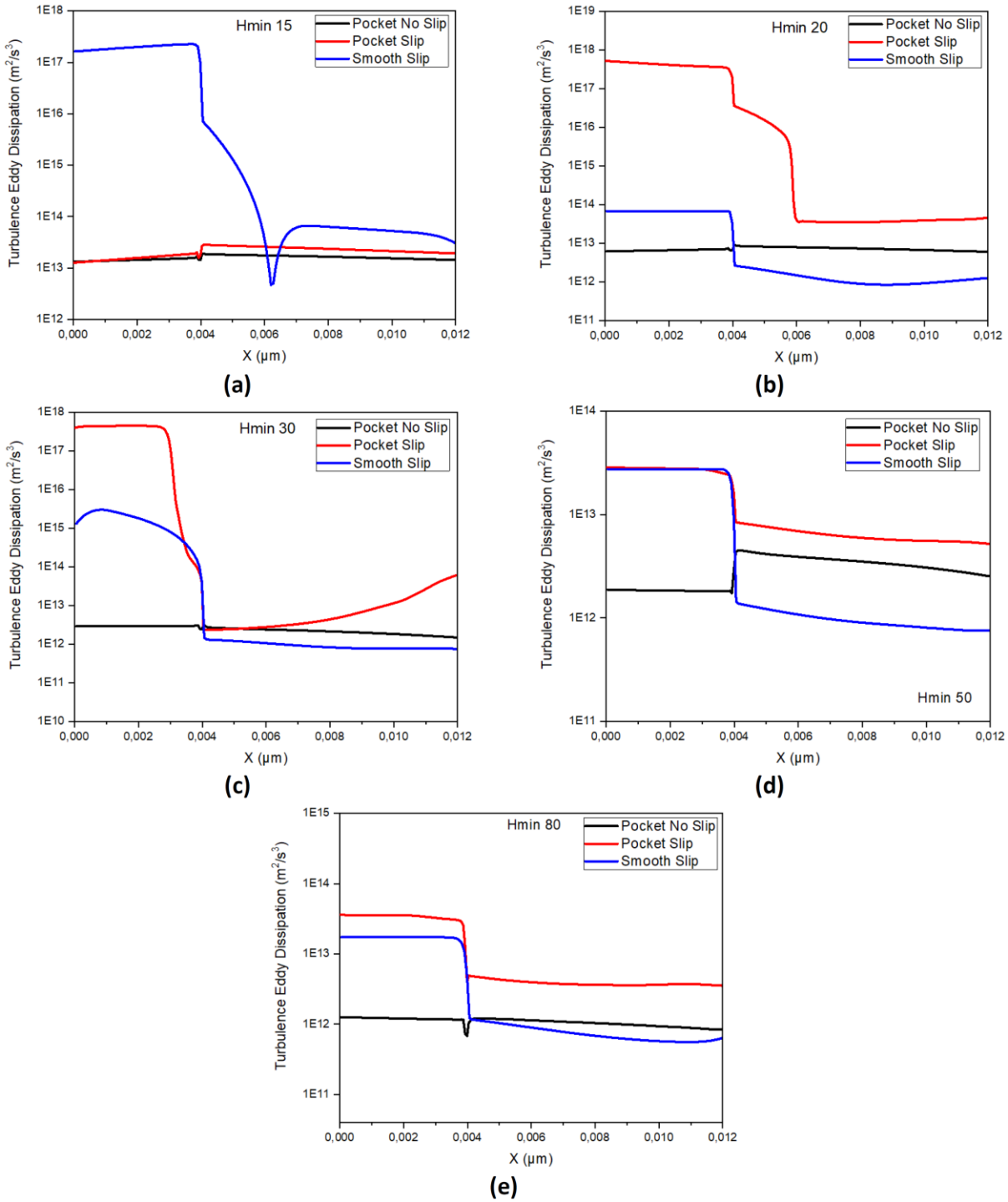

Fig. 14. The TED comparison of H_{min} 15, 20, 30, 50, and 80 μm

In contrast to the phenomenon of decreasing TED after entering into the pocket, there is an increase in TED after entering the pocket in some cases. Furthermore, APL, TKE, and TED increased significantly after entering the pocket area at H_{min} 50 in the pocket no slip model, as shown in Figures 8(d), 11(d), and 14(d). In other words, the existence of this phenomenon confirms that depending on the thickness of the film layer, providing slip can reduce or increase APL, TKE, and TED. For example, in the smooth slip model with H_{min} 15, there was a drastic decrease from 2.26E+17 m^2/s^3 when it entered the slip area, then decreased and stabilized around 5.34E+13 m^2/s^3. However, in the pocket slip model at H_{min} 50, the value has increased from 3.17E+12 m^2/s^3 to a steady state in the range of 2.01E+12 m^2/s^3. In general, slip engineered can reduce TED.

The average TED in the three models is shown in Figure 15. The no slip pocket model, like the average trend of APL and TKE, has the smallest TED value at H_{min} 80, which is 1.011E+12 m^2/s^3. Meanwhile, when compared to other models, the smooth slip model on H_{min} 20 has the highest value, 4.449E+17 m^2/s^3. Furthermore, it should be noted that the smooth slip model H_{min} 15 has lower TED and TKE values than H_{min} 20, but not APL. At H_{min} 50, the average APL values of the three models are very close. This means that the thrust bearing models have almost no effect on the average APL at H_{min} 50. In general, as TKE decreases (see Figure 12), the fluctuation of lubricant velocity and subsequent bearing noise diminishes. The small TKE causes the TED to decrease.

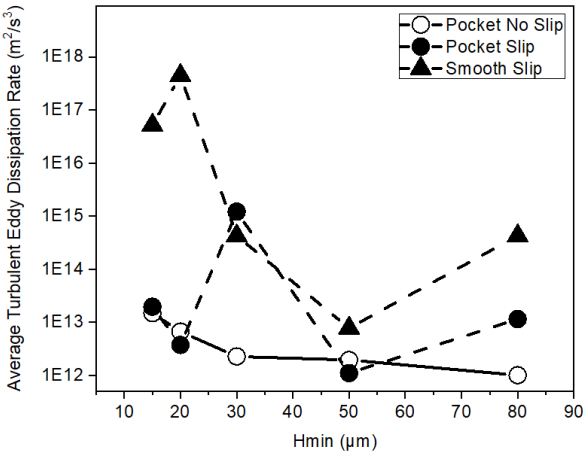

Fig. 15. The average TED rate comparison of H_{min} 15, 20, 30, 50, and 80 μm of pocket no slip, pocket slip, and smooth slip models

4. Conclusions

The effect of providing slip on the pocket thrust bearings on APL was examined. In addition, this research compares pocket and conventional bearings, with slip engineered in the pocket and the same area of the smooth surface bearing. To evaluate the performance of bearings with slip engineered, a bearing with no slip conditions is created. The TKE and TED rate were also examined with the APL, using numerical research with minimal film thickness variations. The conclusion is as follows:

i. Slip engineered in the pocketed and smooth surface bearings has been shown to provide benefits by lowering the value of APL, TKE, and TED.
ii. The TKE is directly proportional to APL, the higher the APL, the higher the TKE value. Among the three models, pocket no slip was found to be the most "stable" in noise at a variety of film thicknesses. Meanwhile, compared to the other models, the smooth slip model has the lowest noise.

iii. The use of a pocket on the bearing has been verified to reduce both APL and TKE. Compared to other models, the pocket no slip model has the lowest average for both APL and TKE.

iv. At a low film thickness (H_{min} 15), pocket slip and pocket no slip have no significant noise reduction effect in pocket models. However, it can reduce noise by up to 60% in the smooth slip model.

v. For all models, the average value of APL, TKE, and TED at large film thickness (H_{min} 80) is the smallest.

All thrust bearing models are independent of cavitation. In the future, it is recommended to model closed pocket thrust bearings with cavitation to examine their influence on slip modelling.

Acknowledgement
This research was not funded by any grant.

References

[1] Etsion, Izhak, G. Halperin, V. Brizmer, and Y. Kligerman. "Experimental investigation of laser surface textured parallel thrust bearings." *Tribology Letters* 17, no. 2 (2004): 295-300. https://doi.org/10.1023/B:TRIL.0000032467.88800.59

[2] Henry, Y., J. Bouyer, and M. Fillon. "An experimental analysis of the hydrodynamic contribution of textured thrust bearings during steady-state operation: A comparison with the untextured parallel surface configuration." *Proceedings of the Institution of Mechanical Engineers, Part J: Journal of Engineering Tribology* 229, no. 4 (2015): 362-375. https://doi.org/10.1177/1350650114537484

[3] Marian, Victor Gabriel, Dumitru Gabriel, Gunter Knoll, and Salvatore Filippone. "Theoretical and experimental analysis of a laser textured thrust bearing." *Tribology letters* 44 (2011): 335-343. https://doi.org/10.1007/s11249-011-9857-8

[4] Fouflias, Dimitrios G., Anastassios G. Charitopoulos, Christos I. Papadopoulos, Lambros Kaiktsis, and Michel Fillon. "Performance comparison between textured, pocket, and tapered-land sector-pad thrust bearings using computational fluid dynamics thermohydrodynamic analysis." *Proceedings of the Institution of Mechanical Engineers, Part J: Journal of Engineering Tribology* 229, no. 4 (2015): 376-397. https://doi.org/10.1177/1350650114550346

[5] Zouzoulas, Vassilios, and Christos I. Papadopoulos. "3-D thermohydrodynamic analysis of textured, grooved, pocketed and hydrophobic pivoted-pad thrust bearings." *Tribology International* 110 (2017): 426-440. https://doi.org/10.1016/j.triboint.2016.10.001

[6] Zhang, Jinyu, and Yonggang Meng. "Direct observation of cavitation phenomenon and hydrodynamic lubrication analysis of textured surfaces." *Tribology Letters* 46 (2012): 147-158. https://doi.org/10.1007/s11249-012-9935-6

[7] Novotný, Pavel, Martin Jonák, and Jiří Vacula. "Evolutionary optimisation of the thrust bearing considering multiple operating conditions in turbomachinery." *International Journal of Mechanical Sciences* 195 (2021): 106240. https://doi.org/10.1016/j.ijmecsci.2020.106240

[8] Wos, Slawomir, Waldemar Koszela, and Pawel Pawlus. "Determination of oil demand for textured surfaces under conformal contact conditions." *Tribology International* 93 (2016): 602-613. https://doi.org/10.1016/j.triboint.2015.05.016

[9] Wang, Xiaolei, Wei Liu, Fei Zhou, and Di Zhu. "Preliminary investigation of the effect of dimple size on friction in line contacts." *Tribology International* 42, no. 7 (2009): 1118-1123. https://doi.org/10.1016/j.triboint.2009.03.012

[10] Kumar, Vivek, and Satish C. Sharma. "Influence of dimple geometry and micro-roughness orientation on performance of textured hybrid thrust pad bearing." *Meccanica* 53 (2018): 3579-3606. https://doi.org/10.1007/s11012-018-0897-0

[11] Ryk, G., and It Etsion. "Testing piston rings with partial laser surface texturing for friction reduction." *Wear* 261, no. 7-8 (2006): 792-796. https://doi.org/10.1016/j.wear.2006.01.031

[12] Wang, Xiaolei, Koji Kato, Koshi Adachi, and Kohji Aizawa. "The effect of laser texturing of SiC surface on the critical load for the transition of water lubrication mode from hydrodynamic to mixed." *Tribology International* 34, no. 10 (2001): 703-711. https://doi.org/10.1016/S0301-679X(01)00063-9

[13] Wang, Xiaolei, Koji Kato, and Koshi Adachi. "The lubrication effect of micro-pits on parallel sliding faces of SiC in water." *Tribology transactions* 45, no. 3 (2002): 294-301. https://doi.org/10.1080/10402000208982552
[14] Rahmani, Ramin, Ayoub Shirvani, and Hassan Shirvani. "Optimization of partially textured parallel thrust bearings with square-shaped micro-dimples." *Tribology Transactions* 50, no. 3 (2007): 401-406. https://doi.org/10.1080/10402000701429261
[15] Shen, Cong, and M. M. Khonsari. "Effect of dimple's internal structure on hydrodynamic lubrication." *Tribology Letters* 52 (2013): 415-430. https://doi.org/10.1007/s11249-013-0225-8
[16] Vakilian, M., Seyyed Abdolreza Gandjalikhan Nassab, and Z. Kheirandish. "Study of inertia effect on thermohydrodynamic characteristics of Rayleigh step bearings by CFD method." *Mechanics & Industry* 14, no. 4 (2013): 275-285. https://doi.org/10.1051/meca/2013065
[17] Wodtke, Michał, Artur Olszewski, and Michał Wasilczuk. "Application of the fluid–structure interaction technique for the analysis of hydrodynamic lubrication problems." *Proceedings of the Institution of Mechanical Engineers, Part J: Journal of Engineering Tribology* 227, no. 8 (2013): 888-897. https://doi.org/10.1177/1350650113481147
[18] Papadopoulos, C. I., L. Kaiktsis, and M. Fillon. "Computational fluid dynamics thermohydrodynamic analysis of three-dimensional sector-pad thrust bearings with rectangular dimples." *Journal of Tribology* 136, no. 1 (2014): 011702. https://doi.org/10.1115/1.4025245
[19] Song, Yin, Xiao Ren, Chun-wei Gu, and Xue-song Li. "Experimental and numerical studies of cavitation effects in a tapered land thrust bearing." *Journal of Tribology* 137, no. 1 (2015). https://doi.org/10.1115/1.4028264
[20] Ghani, Jaharah A., Faarih Farhan Mohd Nasir, Haniff Abdul Rahman, Wan Fathul Hakim Wan Zamri, Mohd Shahir Kasim, and Shalina Sheikh Muhamad. "Computational fluid dynamic analysis on tribological performance under hydrodynamic lubrication of dimple textured surface produced using turning process." *Wear* 477 (2021): 203898. https://doi.org/10.1016/j.wear.2021.203898
[21] Zhai, Liming, Yongyao Luo, Zhengwei Wang, and Xin Liu. "3D Two-way coupled TEHD analysis on the lubricating characteristics of thrust bearings in pump-turbine units by combining CFD and FEA." *Chinese Journal of Mechanical Engineering* 29, no. 1 (2016): 112-123. https://doi.org/10.3901/CJME.2015.0922.113
[22] Zhai, Liming, Zhengwei Wang, Yongyao Luo, and Zhongjie Li. "TEHD analysis of a bidirectional thrust bearing in a pumped storage unit." *Industrial Lubrication and Tribology* (2016). https://doi.org/10.1108/ILT-07-2015-0092
[23] Salant, Richard F., and Alicia E. Fortier. "Numerical analysis of a slider bearing with a heterogeneous slip/no-slip surface." *Tribology Transactions* 47, no. 3 (2004): 328-334. https://doi.org/10.1080/05698190490455348
[24] Tauviqirrahman, Mohammad, Rifky Ismail, Jamari Jamari, and Dirk J. Schipper. "Combined effect of texturing and boundary slippage in lubricated sliding contacts." *Tribology international* 66 (2013): 274-281. https://doi.org/10.1016/j.triboint.2013.05.014
[25] Wang, Yun-Lei, Jiu-Hui Wu, Mu-Ming Hao, and Lu-Shuai Xu. "Improved hydrodynamic performance of liquid film seal by considering boundary slip and cavitation." *Industrial Lubrication and Tribology* 71, no. 9 (2019): 1108-1115. https://doi.org/10.1108/ILT-03-2019-0088
[26] Zhu, B., Y. P. Li, W. G. Wang, and M. K. Lei. "Boundary slippage modeling and optimization of hydrophobic tilting pad thrust bearing with elastic deformation." *Tribology International* 136 (2019): 299-316. https://doi.org/10.1016/j.triboint.2019.03.060
[27] Jamari, Jamari, M. Muchammad, F. Hilmy, and Muhammad Tauviqirrahman. "Effect of inertia on the cavitation phenomena of hydrodynamic textured bearings considering slip." *Journal of the Brazilian Society of Mechanical Sciences and Engineering* 41 (2019): 1-14. https://doi.org/10.1007/s40430-019-1890-9
[28] Tauviqirrahman, Mohammad, J. Jamari, Arjuno Aryo Wicaksono, M. Muchammad, S. Susilowati, Yustina Ngatilah, and Caecilia Pujiastuti. "CFD analysis of journal bearing with a heterogeneous rough/smooth surface." *Lubricants* 9, no. 9 (2021): 88. https://doi.org/10.3390/lubricants9090088
[29] Lu, Xiaobin, and M. M. Khonsari. "An experimental investigation of dimple effect on the stribeck curve of journal bearings." *Tribology letters* 27 (2007): 169-176. https://doi.org/10.1007/s11249-007-9217-x
[30] Meng, F. M., and W. Zhang. "Effects of compound groove texture on noise of journal bearing." *Journal of Tribology* 140, no. 3 (2018). https://doi.org/10.1115/1.4038353
[31] Meng, Fanming, Zhang Wei, Du Minggang, and Guixiang Gao. "Study of acoustic performance of textured journal bearing." *Proceedings of the Institution of Mechanical Engineers, Part J: Journal of Engineering Tribology* 230, no. 2 (2016): 156-169. https://doi.org/10.1177/1350650115594406
[32] Meng, Fanming, Ruihong Shu, and Lin Chen. "Influences of operation parameters on noise of journal bearing with compound texture considering lubricant thermal effect." *Proceedings of the Institution of Mechanical Engineers, Part J: Journal of Engineering Tribology* 234, no. 7 (2020): 991-1006. https://doi.org/10.1177/1350650119868910
[33] Muchammad, M., M. Tauviqirrahman, L. Mario, and J. Jamari. "Thermo-hydrodynamic analysis of multistep texture effect on the performance of journal bearings through acoustic and tribological characteristics." *Journal of the*

Brazilian Society of Mechanical Sciences and Engineering 44, no. 7 (2022): 310. https://doi.org/10.1007/s40430-022-03622-8

[34] Tauviqirrahman, Mohammad, M. Fadhli Afif, P. Paryanto, J. Jamari, and Wahyu Caesarendra. "Investigation of the tribological performance of heterogeneous slip/no-slip journal bearing considering thermo-hydrodynamic effects." *Fluids* 6, no. 2 (2021): 48. https://doi.org/10.3390/fluids6020048

[35] Tauviqirrahman, Mohammad, J. Jamari, Muhammad Bagir, Wahyu Caesarendra, and P. Paryanto. "Elastohydrodynamic behavior analysis on water-lubricated journal bearing: a study of acoustic and tribological performance based on CFD-FSI approach." *Journal of the Brazilian Society of Mechanical Sciences and Engineering* 44 (2022): 1-19. https://doi.org/10.1007/s40430-021-03314-9

[36] Sahlin, Fredrik, Sergei B. Glavatskih, Torbjo¨ rn Almqvist, and Roland Larsson. "Two-dimensional CFD-analysis of micro-patterned surfaces in hydrodynamic lubrication." *J. Trib.* 127, no. 1 (2005): 96-102. https://doi.org/10.1115/1.1828067

[37] Ansys, I. "ANSYS Fluent 18.2 user's manual." *ANSYS Canonsburg, PA* (2017).